NASA Technical Memorandum 102561

Theory and Experimental Technique for Nondestructive Evaluation of Ceramic Composites

Edward R. Generazio
Lewis Research Center
Cleveland, Ohio

Prepared for the
March Meeting of the American Society
for Nondestructive Testing
Columbus, Ohio, March 15, 1990

NASA

THEORY AND EXPERIMENTAL TECHNIQUE FOR NONDESTRUCTIVE EVALUATION OF CERAMIC COMPOSITES

Edward R. Generazio
National Aeronautics and Space Administration
Lewis Research Center
Cleveland, Ohio 44135

SUMMARY

The important ultrasonic scattering mechanisms for SiC and Si_3N_4 ceramic composites have been identified by examining the interaction of ultrasound with individual fibers, pores, and grains. The dominant scattering mechanisms have been identified as asymmetric refractive scattering due to porosity gradients in the matrix material, and symmetric diffractive scattering at the fiber-to-matrix interface and at individual pores. The effect of the ultrasonic reflection coefficient and surface roughness on the ultrasonic evaluation has been highlighted. A new nonintrusive ultrasonic evaluation technique, the angular power spectrum scan (APSS), has been presented that is sensitive to microstructural variations in composites. Preliminary results indicate that the APSS will yield information on the composite microstructure that is not available by any other nondestructive technique.

INTRODUCTION

Advanced high-temperature ceramics (ref. 1) are being developed for use in the next generation of aerospace systems. Recently, considerable attention has been given to monolithic SiC and Si_3N_4 (ref. 2) for these high-temperature applications. Research on monolithic ceramics subsequently led to the current developmental research on advanced high-temperature ceramic composites. These composites consist of particles, whiskers, or fibers in ceramic matrices. A variety of processing techniques are being investigated in an effort to produce high-temperature composites with optimized thermal and mechanical properties. Plasma spraying, reaction bonding, slurry pressing, and sintering are typical techniques used to produce high-temperature ceramics. These processes often result in a composite that has a wide variability in microstructure. Typically, microstructural variations such as porosity, agglomerates, grain size, interfacial structure between phases, and orientation of phases all play a role in determining the materials properties. The importance and effects of these and other microstructural variations on the composite materials' thermal and mechanical properties are being aggressively researched (refs. 1 to 8).

Ultrasonic C-scans and conventional x-ray radiography are routinely performed for nondestructive evaluation of a variety of materials. These NDE techniques reveal macroscopic internal features such as delaminations, debonds, porosity, and cracks. Each of these features is important when considering the use of the tested material where strength and integrity must be assured. However, standard ultrasonic C-scans and conventional x-ray radiography cannot be expected to characterize the crucial minute variations in the ceramic microstructure that affect strength and toughness. For example, the characterization of toughness limiting matrix-second phase interface is beyond the capability of these standard techniques. Advanced NDE technologies can be expected

to nonintrusively evaluate the second phase to matrix interface in composites. The goal of this work is to move NDE technologies in the direction required for assisting in the development of advanced ceramics. The preliminary results shown here indicate that an advanced ultrasonic scanning technique and analysis will be required for these composite systems. A new nonintrusive ultrasonic evaluation technique called the angular power spectrum scan (APSS) is discussed.

SYMBOLS

APS	angular power spectrum
APSS	angular power spectrum scan
A_f	final amplitude
A_o	ultrasonic wave of known amplitude
a	distance between adjacent fiber edges
a'	pore diameter
BCS	buffer rod-couplant-sample
$B_{1,2,3}$	back surface echoes
d	distance between fiber centers
FS	front surface
I_o	intensity at $x = 0$ or $r = 0$
J	Bessel function
N	number of fibers
PASS	precision acoustic scanning system
p	degree of fiber opacity
R_b	back reflection coefficient
R_f	front reflection coefficient
r	radial distance from beam axis on the image plane
S	complex wave speed
S/N	signal-to-noise ratio of the input ultrasonic pulse
x	sample thickness
x'	distance perpendicular to fiber axis on the image plane

z distance between pore, or fiber, and the image plane

α measured attenuation

θ polar angle

θ' angle of incidence

λ wavelength

σ variance

σ_α uncertainty in attenuation measurement

ϕ azimuthal angle

Subscripts

L incident wave

m medium through which wave propagates

1L longitudinal incident wave

1n longitudinal wave propagation

2L shear incident wave

2n shear wave propagation

BACKGROUND

Ultrasonic imaging can be done by means of several techniques. The most common is the one used by commercially available ultrasonic immersion C-scanning systems. An ultrasonic wave of known amplitude A_o is transmitted through a sample as shown in figure 1. The final amplitude A_f, or C-scan image, is a representation of relative attenuation, or energy lost, by the ultrasonic wave as it traverses through the sample. Unfortunately, C-scan images are not true representations of the energy lost by the ultrasonic wave as it travels through the sample. The ultrasonic reflection coefficients at the water-to-sample interfaces are not generally imaged. These reflection coefficients are large and must be included in the analysis for determination of the attenuation. The reflection coefficient is used to determine the accuracy of an acoustic image. It can also be used to determine the most accurate acoustic imaging technique to use.

In order to obtain the reflection coefficient at the back surface, a modified two-transducer arrangement must be used (fig. 2) where the transducers are both transmitters and receivers. The variance σ_α in the attenuation measurement for this immersion arrangement is given by reference 9

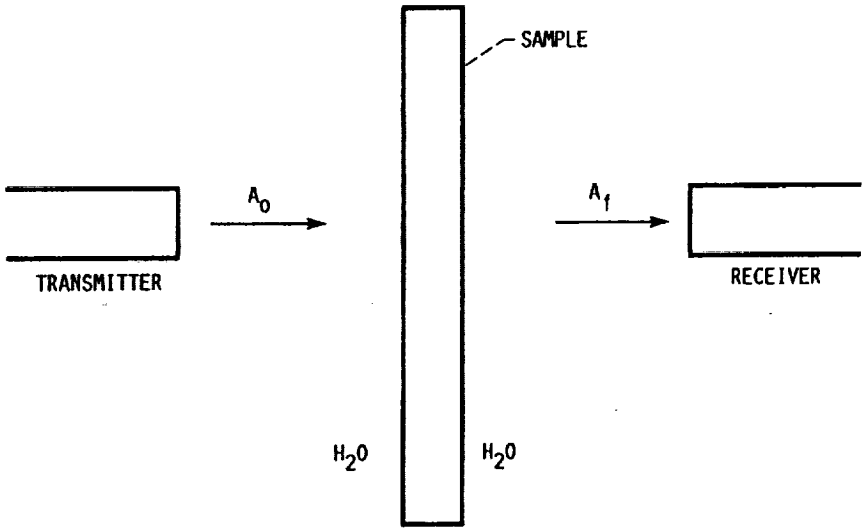

FIGURE 1. - STANDARD IMMERSION ULTRASONIC C-SCANNING ARRANGEMENT.

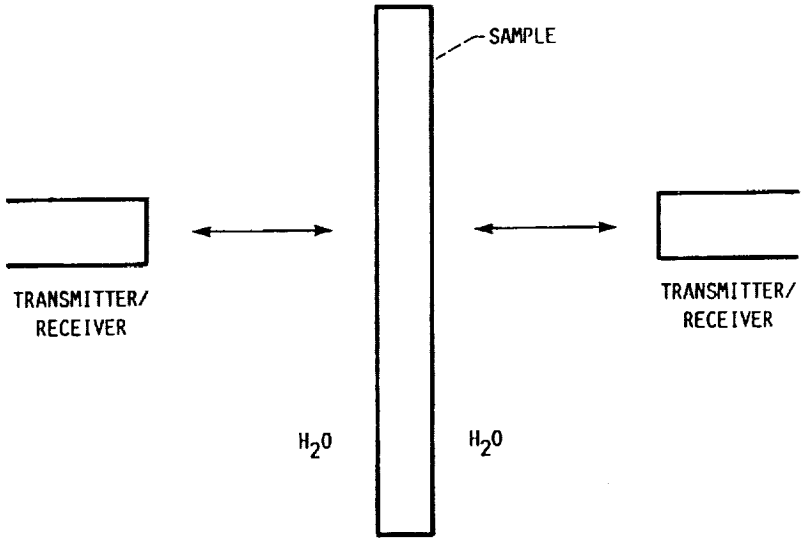

FIGURE 2. - MODIFIED IMMERSION ULTRASONIC SCANNING ARRANGEMENT NEEDED TO DETERMINE REFLECTION COEFFICIENTS AT FRONT AND BACK SURFACES. ULTRASONIC WAVE OF KNOWN AMPLITUDE, A_0; FINAL AMPLITUDE, A_f.

$$\left(\frac{\sigma_\alpha}{\alpha}\right)\left(\frac{S}{N}\right) = \frac{1}{2\alpha x}\left[\frac{\left(1 - R_b^2\right)^2\left[\left(1 + R_f^2\right)^2 + 4R_f^2\right]}{\left(1 - R_f^2\right)^2\left(1 - R_b^2\right)^2} + \frac{\left(1 - R_f^2\right)^2\left[\left(1 + R_b^2\right) + 4R_b^2\right]}{\left(1 - R_f^2\right)^2\left(1 - R_b^2\right)^2}\right.$$

$$\left. + \frac{2\left(1 - R_f^2\right)\left(1 + R_b^2\right)e^{2\alpha x}}{\left(1 - R_f^2\right)^2\left(1 - R_b^2\right)^2}\right]^{1/2} \qquad (1)$$

where S/N is the signal-to-noise ratio of the input ultrasonic pulse, α is the measured attenuation, R_f and R_b are the reflection coefficient magnitudes on the front and back surface of the sample, respectively, and x is the sample thickness.

Ceramics generally have immersion reflection coefficients of about 0.92. This corresponds to an uncertainty of about 15 to 30 percent. If we are to understand the interaction of ultrasonic waves with ceramics systems, we need the most accurate evaluation technique available.

An alternative technique to immersion scanning is contact scanning. This technique uses a precision acoustic scanning system (PASS) that is described in detail elsewhere (refs. 10 to 13). Briefly, a single transducer is used to make precise and accurate attenuation measurements. The experimental arrangement for contact ultrasonic measurements is shown in figure 3. An ultrasonic wave is introduced into the sample via the buffer rod-couplant-sample (BCS) interface. The ultrasonic wave subsequently echoes within the sample. By measuring the reflection coefficient R_f (ref. 12) at the BCS interface and

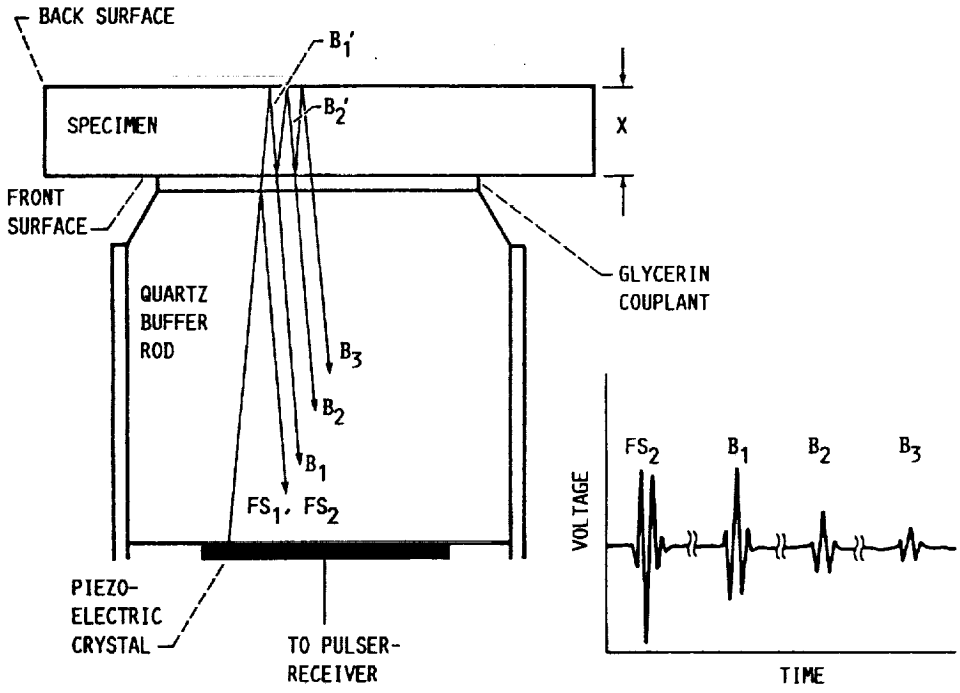

FIGURE 3. - CONFIGURATION FOR CONTACT ULTRASONIC MEASUREMENTS.

the appropriate echoes, the ultrasonic attenuation can be determined. The variance in the attenuation measurement for this arrangement is given by reference 12:

$$\left(\frac{\sigma_\alpha}{\alpha}\right)\left(\frac{S}{N}\right) = \frac{1}{2\alpha x}\left[\frac{\left[R_f^2 R_b^2 + e^{4\alpha x}\right]e^{4\alpha x}}{\left(1 - R_f^2\right)^2} + R_b^4 + R_f^2 R_b^2 \quad \frac{1}{R_b^4 R_f^2} + 2\right]^{1/2} \tag{2}$$

Note that the sample need not be air-backed. That is, R_b may be <1. Ceramics generally have contact reflection coefficients of about 0.5. This corresponds to a variance of about 7 to 15 percent.

Equations (1) and (2) are graphically shown in figure 4. The configuration having the lowest variance values obtained from equations (1) and (2) is shown. The solid line in the figure can be used to make a decision about which technique should be applied for a particular experimental sample. Above the solid line, a precision contact pulse-echo measurement is preferred. Below the solid line, an immersion through transmission yields the least uncertainty in the attenuation measurement.

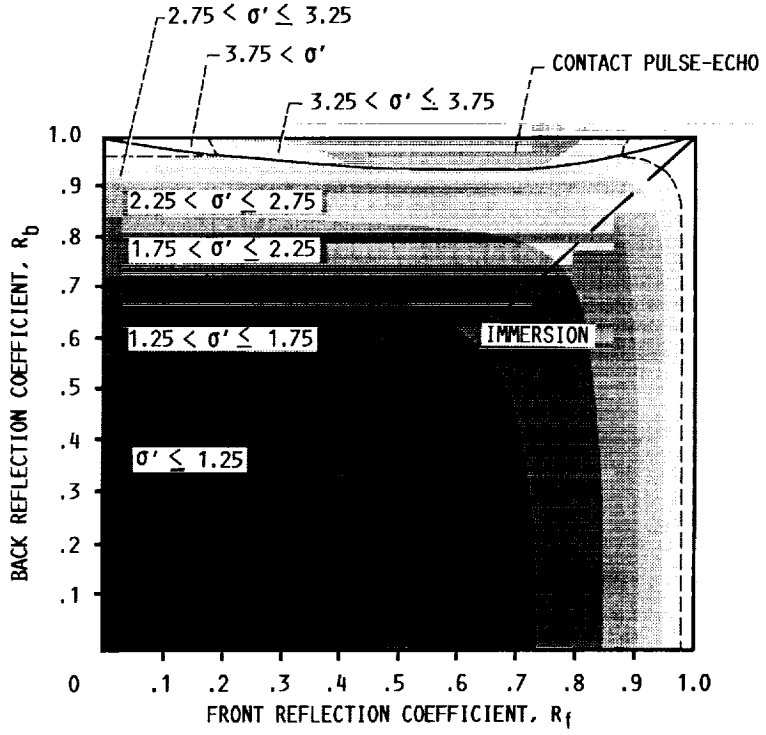

FIGURE 4. - UNCERTAINTY IN ATTENUATION AS FUNCTION OF FRONT AND BACK SURFACE REFLECTION COEFFICIENTS FOR BOTH IMMERSION AND CONTACT ULTRASONIC SCANNING. CONTACT SCANNING METHOD IS MORE ACCURATE ABOVE THE SOLID LINE. LONG-DASHED LINE INDICATES THE UNCERTAINTY FOR THE IMMERSION ARRANGEMENT WHERE THE SAMPLE HAS IDENTICAL REFLECTION COEFFICIENTS ON BOTH SIDES. HERE $2\alpha X$ = 1, α = 1, AND σ' = LOG $[\sigma_\alpha/\alpha(S/N)]$.

Immersion ultrasonic systems generally have similar reflection coefficients for R_f and R_b. The variance is symmetric with respect to the $R_f = R_b$ axis for immersion measurements. The long dashed line in figure 4 indicates the path used to determine the variance. The stated reflection coefficients are for acoustically flat (i.e., flat when compared with the ultrasonic wavelength) specimens. Any additional roughness will further increase the reflection coefficient. Many solid materials will fit on this curve between 0.84 and 0.97.

Figure 5 shows the variance for PMMA, PMC, Al, Pb, SiC, Al_3O_2, Ni, W, and Si_3N_4 for both immersion ($R_f = R_b$) and contact ultrasonic methods. When evaluating Ni, SiC, Si_3N_4, Al_3O_2, and W, the contact pulse-echo method yields the least uncertain and most accurate attenuation measurement. Therefore, contact scanning should be, and is, used here for evaluating the monolithic ceramic matrix material.

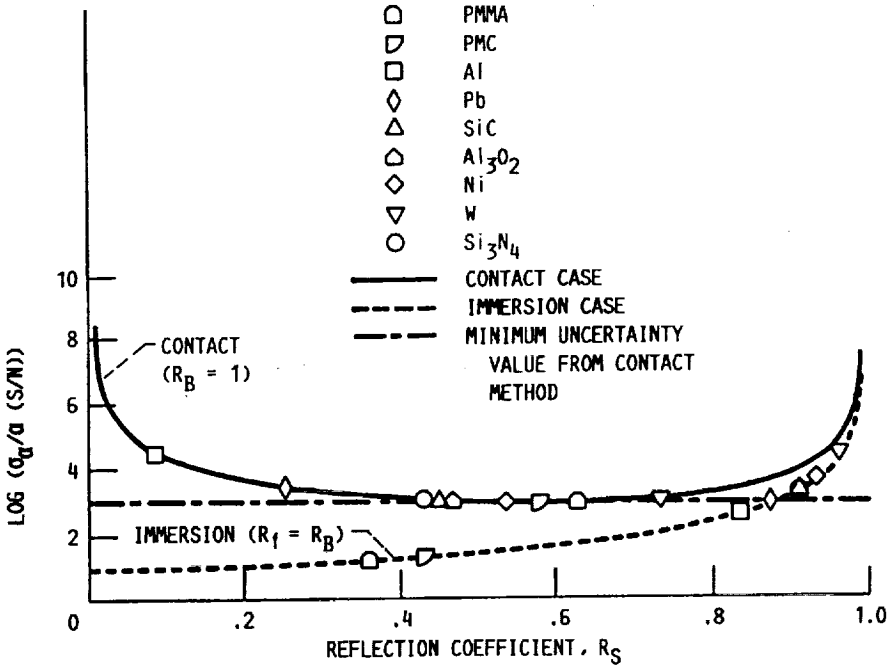

FIGURE 5. - UNCERTAINTY COMPARISON FOR SEVERAL MATERIALS. FOR Al_3O_2, Ni, W, SiC, AND Si_3N_4 THE UNCERTAINTY IS LOWER WHEN USING A CONTACT SCANNING METHOD. THE CURVES ARE GENERATED FROM EQUATIONS 1 AND 2. THE DASHED LINE IS FOR THE IMMERSION CASE. THE SOLID LINE IS FOR THE CONTACT CASE. THE DASHED-DOTTED LINE INDICATES THE MINIMUM UNCERTAINTY VALUE THAT THE CONTACT METHOD CAN YIELD. HERE $2\alpha X = 1$, $a = 1$, AND $\sigma' = \text{LOG } [\sigma_a/a(S/N)]$.

APPROACH

Ultrasonic evaluation of composites may be approached from two directions. The complete composite system can be interrogated as a whole system. The resultant ultrasonic signals are complicated and difficult to interpret. Since the actual mechanisms that are forming these signals remain unknown, their interpretation is subject to question. An alternative to this approach is to explicitly determine the interaction of ultrasound with each individual

component, or phase, of the composite. This information is then used for formulating theories that explain the ultrasonic signals obtained from the full composite system. The latter approach is used for this work.

SCATTERING DUE TO GRAIN BOUNDARIES

The matrix materials SiC and Si_3N_4 are acoustically similar; that is, they have similar but not identical densities, ultrasonic velocities, ultrasonic attenuation, and elastic moduli (see table I). The ultrasonic attenuation (for frequencies below 50 MHz) due to grain boundary scattering has been found to be negligible for nearly fully dense SiC and Si_3N_4 having grain sizes less than 15 μm (refs. 11 and 12). Therefore, grain boundary scattering need not be considered for SiC and Si_3N_4 matrix material.

TABLE I

Material	Density, g/cc	Young's modulus, GPa	Velocity, cm/μsec	Attenuation, N/cm, 50 MHz
SiC	3.12	440	1.22	<0.1
Si_3N_4	3.28	310	1.09	<0.1

SCATTERING DUE TO PORES

The interaction of ultrasonic waves with individual pores is well understood. When an ultrasonic wave interacts with a pore, a spherical wave is generated at the pore site. The spherical wave interacts with the main beam to form a diffraction pattern. The intensity observed at the plane perpendicular to the sound direction is given by the relation (ref. 14)

$$I = I_o\left[\frac{a'}{r} J_1\left(\frac{2\pi a' r}{\lambda z}\right)\right]^2 \tag{3}$$

where J_1 is the Bessel function, a' is the pore diameter, z is the distance between the pore and the image plane, r is the radial distance from the beam axis on the image plane, and I_o is the intensity at $r = 0$.

The spherical wave and diffraction pattern are observable by many ultrasonic imaging techniques. The ultrasonic surface wave and longitudinal wave images in figure 6 reveal the spherical wave and spherical diffraction pattern, respectively, from a single subsurface pore. The ultrasonic energy is symmetrically scattered to form a cylindrically symmetric pattern on a plane perpendicular to the beam axis.

A composite generally has many pores dispersed throughout the matrix. The energy scattered from these pores is not observable as individual ring patterns. The patterns overlap and form a uniform cylindrically symmetric intensity background. Increasing the number of pores (with the same diameter) per unit volume will result in an increased amount of scattering per unit volume

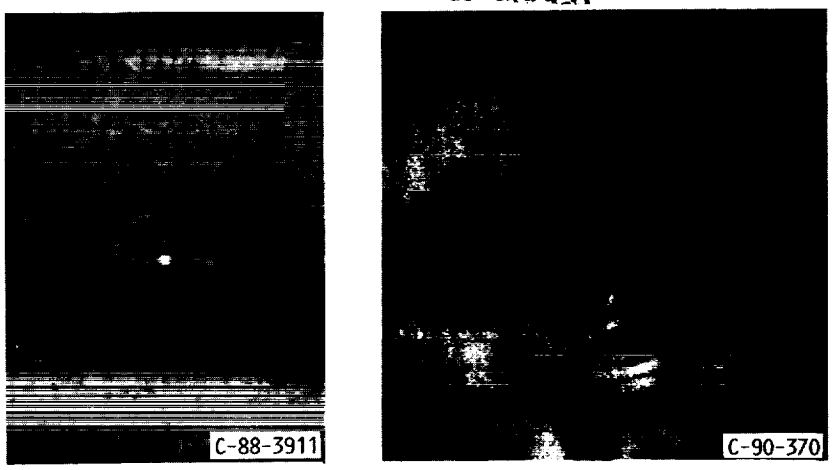

(a) SURFACE WAVE IMAGE REVEALING SUBSURFACE PORE IN SiC.

(b) SCANNING LASER ACOUSTIC MICROSCOPE IMAGE REVEALING A SUBSURFACE PORE IN SiO_2. ONLY THE RIGHT HALF OF THE DIFFRACTION PATTERN IS VISIBLE BECAUSE OF THE EXPERIMENTAL CONFIGURATION.

FIGURE 6. - ULTRASONIC IMAGES OF SUBSURFACE PORES.

and, therefore, a decrease in intensities. It is noted here that partially or incompletely bonded regions between composite lamina are ultrasonically equivalent to regions of increased porosity. Therefore, a cylindrically symmetric decrease in intensity can be due to increased matrix porosity or incomplete interlaminar bonding.

SCATTERING DUE TO POROSITY GRADIENTS

Refraction of waves occurs at boundaries that are velocity mismatched. For planar boundaries between elastic media (e.g., the boundary between medium 1 and medium 2), longitudinal and shear waves are refracted and reflected at the boundary at an angle determined by the well-known Snell's law for elastic media (ref. 15):

$$\sin \psi_{Lmn} = \left[\frac{S_{mn}}{S_{1L}}\right] \sin \theta'_{1L} \tag{4}$$

where θ' and ψ are the angles measured from the surface normal vector (θ' is also the incident angle), and S is the complex wave speed. The subscript L corresponds to longitudinal ($L = 1$) or shear ($L = 2$) incident wave. The subscript m indicates which medium, 1 or 2, the wave is propagating through. The subscript n denotes longitudinal ($n = 1$) or shear ($n = 2$) wave propagation.

The ultrasonic velocity and attenuation images for a specimen of SiC are shown in figure 7. The ultrasonic velocity in porous media is linearly related to the density (ref. 16). The high velocity region in the upper left of the figure corresponds to a high density region. The high attenuation band in the attenuation image is of particular interest. This high attenuation band occurs at the density gradient boundary existing between high and low density regions.

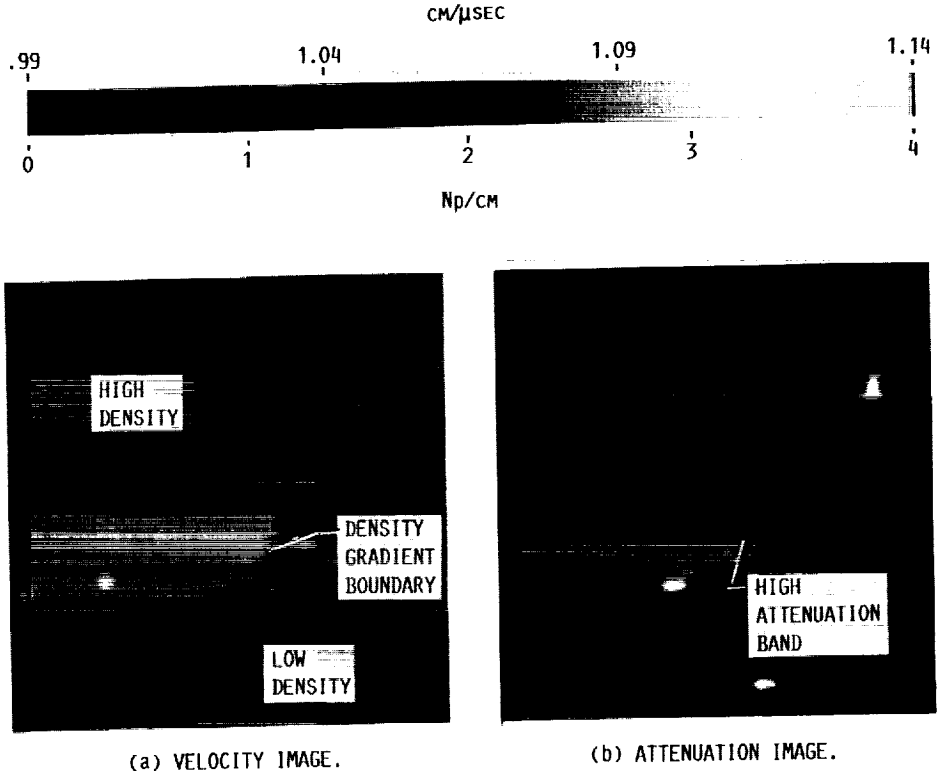

(a) VELOCITY IMAGE. (b) ATTENUATION IMAGE.

FIGURE 7. - ULTRASONIC VELOCITY AND ATTENUATION IMAGES FOR SiC OBTAINED BY PRECISION ACOUSTIC SCANNING SYSTEM (PASS).

The velocity gradients yield high attenuation due to refractive scattering at this boundary. That is, the acoustic energy is being redirected, because of refraction and reflection, from the main acoustic beam. Therefore, regions of high attenuation may indicate the presence of density gradients and not necessarily flaws. Refractive scattering is, in general, asymmetric with respect to the initial direction, or beam axis; that is, if energy is refractively scattered off at an angle $+\psi$, then energy will not, simultaneously, be scattered off at the symmetric angle $-\psi$.

SCATTERING DUE TO FIBERS

The interaction of ultrasound with continuous fibers is analogous to the interaction of light with slit-shaped apertures. The intensity of the scattered wave from a set of parallel fibers embedded in a matrix is given by reference 17,

$$I = I_o\left[\frac{\sin^2\beta}{\beta^2}\right]\left[\frac{\sin^2 N\gamma}{\sin^2\gamma}\right] \qquad \beta = \frac{\pi a}{\lambda}\sin\varepsilon, \qquad \gamma = \frac{\pi d \sin\varepsilon}{\lambda} \qquad \varepsilon = \tan^{-1}\frac{x'}{z} \qquad (5)$$

where z is the distance between the fiber and the image plane, x' is the distance perpendicular to the fiber axis on the image plane, a is the distance between adjacent fiber edges, d is the distance between fiber centers, N is the number of fibers, and I_o is the intensity at $x = 0$. Here it is assumed that the fibers are acoustically opaque. The wave is transmitted through the

grating via the matrix material between adjacent fibers. If we let $N = 1$ then we have the solution for a single fiber in a matrix.

If the fibers are not acoustically opaque, then the intensity observed has two components. One component is caused by a uniform background (e.g., let the fibers be constructed of material identical to the matrix, and perfectly bonded to the matrix). The other component is caused by a grating (eq. (5)) where the maximum intensity of the diffractive component I_o is replaced by pI_o. The degree of opacity of the fibers p varies between fully opaque ($p = 1$) and fully transmitting ($p = 0$).

The opacity of the fibers embedded in a matrix material is determined by both the fiber material and the degree of bonding between the fiber and the matrix. For example, if the fiber and the matrix are both of the same material and the fiber is perfectly bonded, then $p = 0$ so that no diffraction will occur. If the same fiber is completely disbonded from the matrix, then $p = 1$ and diffraction will occur to yield the maximum possible intensity of the diffractive component, I_o. Alternatively, if the fiber material is different from that of the matrix and is perfectly bonded, then the opacity will always be greater than zero and less than one. That is, diffractive scattering will always occur. A completely disbonded fiber, $p = 1$, will have identical results whether the fiber material is similar or dissimilar to the matrix material.

In order to evaluate the interaction of ultrasound with fibers embedded in a matrix material, a single fiber composite system is used. Figure 8 shows an ultrasonic backscattered image of a single surface-breaking SiC fiber in a Si_3N_4 matrix. The fiber is 1.5 cm long and 140 μm in diameter. In the upper

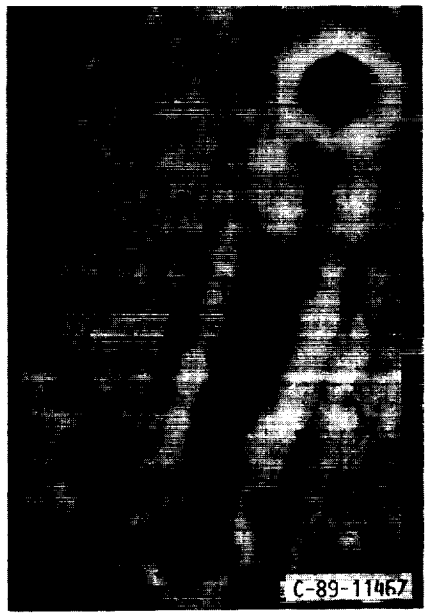

FIGURE 8. - BACKSCATTERED DIFFRACTION PATTERN FROM SINGLE SiC FIBER (1.5 cm LONG, 140 μm DIAM) EMBEDDED IN A Si_3N_4 MATRIX.

part of the figure, the fiber is exposed to the surface and does not show any diffraction effects. The fiber is subsurface in the lower part of the figure and exhibits a strong diffraction effect analogous to an optical single-slit diffraction pattern. The diffraction pattern is symmetric with respect to the fiber axis. The two dark circular areas at the ends of the fiber are regions of microcracking and porosity that formed during the sintering process. The lower subsurface crack zone exhibits a circularly symmetric diffraction pattern similar to that found for subsurface pores (fig. 6).

SUMMARY OF SCATTERING MECHANISMS

The dominant scattering mechanisms for ceramic composites are:

(1) Symmetric diffractive scattering at individual pores
(2) Symmetric diffractive scattering at fibers
(3) Asymmetric refractive scattering at density gradients

Grain boundary scattering has been found to be negligible. The above list of ultrasonic scattering mechanisms can be used to identify an ultrasonic technique for evaluating ceramic composites. The key factor in the above list is the symmetry of the scattered energy. This factor is the main guide in developing an appropriate ultrasonic evaluation technique for ceramic composites.

ANGULAR POWER SPECTRUM

The angular (polar) power spectrum (APS) of the wave transmitted through a composite will contain all the information on each of the above scattering mechanisms. One possible arrangement for determining the angular power spectrum is shown in figure 9(a). The angular power spectrum is obtained at a point by moving the receiver, at a fixed radii, over the half-space containing the transmitted signal. Here the incident wave is transmitted and scattered by the presence of the composite specimen. A receiving transducer is scanned in an angular fashion to determine the energy scattered in the hemisphere described by $-90° \leq \theta \leq 90°$ and $0 \leq \phi < 180°$. This may also be done with either a planar or nonplanar array of transducers or a single or multiple tranducer(s) rotated about the θ and ϕ axes. Many other rotation and array design combinations may be used to determine the APS. The microstructure of the composites varies through the bulk of the specimen; therefore, a scanning arrangement will be required to obtain a complete APSS of the specimen.

Asymmetric components in the APS are indications of porosity or density gradients. The presence of continuous fibers in multidirectional composites will yield power spectrums that are symmetric with respect to the fiber axes. If there are N uniformly spaced fiber directions perpendicular to the incident sound, then the power spectrum will be 2N-fold symmetric with respect to the incident sound direction. The width of the spectrum is a function of angle, ϕ, and is affected by the porosity, the number of fiber layers, the fiber diameter, the distance between the fibers, and the degree of bonding between the fiber and the matrix. The amplitude of the spectrum along the main beam axis indicates the total amount of energy scattered out of the main beam due to all of the above mechanisms.

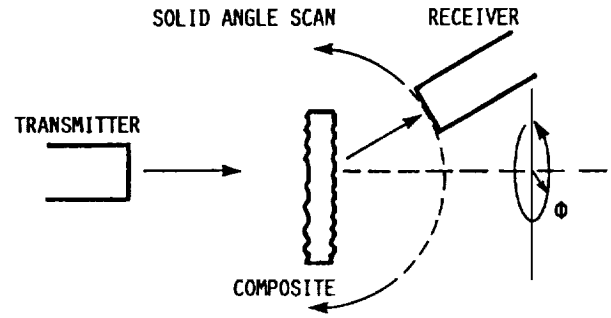

(a) ORIENTATION AND PLACEMENT OF TRANSDUCERS AND SAMPLE TO DETERMINE THE APS.

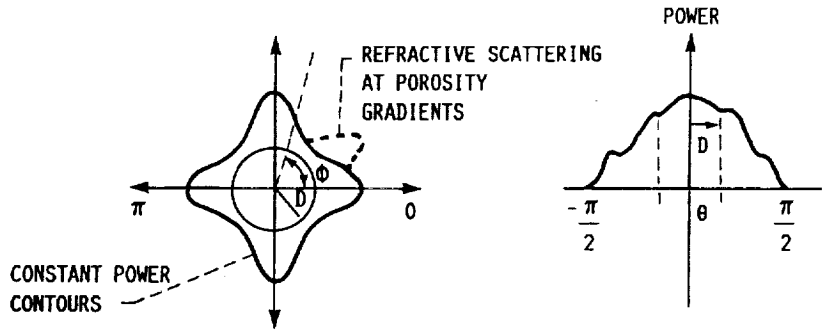

(b) CONSTANT POWER CONTOURS OF APS.

(c) PARTIAL APS (APS AT CONSTANT ANGLE, $\Phi = 0$).

FIGURE 9. - ANGULAR POWER SPECTRUM (APS) OF WAVE TRANSMITTED THROUGH A COMPOSITE.

The interpretation of the APS is best described by examples. Assume that, for a particular composite system, the fiber diameters are uniform, the fiber spacings are uniformly repetitive, and the fiber-to-matrix bond is uniform everywhere. An APS constant power contour level for a 0°/90° composite system should appear as shown in figure 9(b). This APS is four-fold symmetric with respect to the beam axis. A uniform increase (or decrease) in porosity throughout the sample will increase (or decrease) the diameter D of the circularly symmetric constant power component of the APS (figs. 9(b) and (c)). If the bonding between the matrix and the fiber is weakened ($p \to 1$) then the amplitude of the four-fold symmetric diffraction pattern will increase. If there are porosity gradients present, the component of the APS due to porosity will form an asymmetric shape as shown in the dotted curve in figure 9(b).

PRELIMINARY EXPERIMENTAL RESULTS

Two identically produced SiC/SiC laminates with 0°/90° Nicalon fabric composites were used. Conventional radiographic and ultrasonic C-scan images are shown in figure 10 for specimens labeled A and B. The two radiographic images appear similar. Systematic variations in density are observed in both specimens as a series of 0.5-cm-diam dark disks spaced about 1.5 cm apart. These dark regions correspond to high density regions. The fiber weave pattern can also be observed in radiographs.

Ultrasonic C-scans at 10 MHz (fig. 10) reveal quite different results. The ultrasonic image of sample A is more uniform and darker (dark (light) corresponds to poor (good) ultrasonic transmission) than that of sample B. This indicates poor interlaminar bonding in sample A. A very porous system could also produce this type of image. However, the radiographs indicate that the porosity for the two specimens is similar. The ultrasonic image for specimen B has a large amount of fluctuations in the intensity and has the appearance of being blurred.

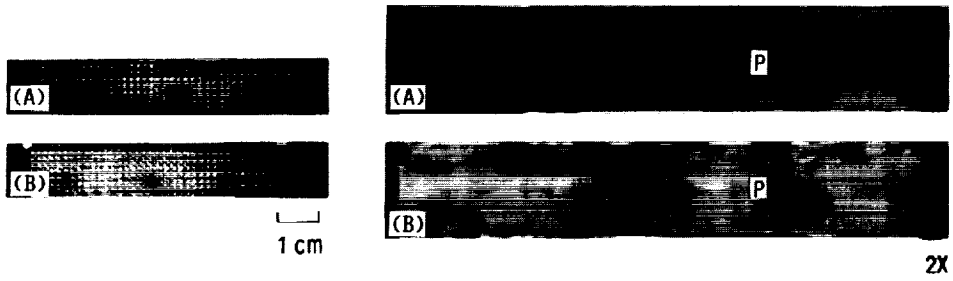

FIGURE 10. - RADIOGRAPHIC AND ULTRASONIC C-SCAN IMAGES.

A complete APSS system has not yet been developed. In lieu of this, a partial APS was done at 10 MHz by holding one angle constant (ϕ = 0°) and $-60° \leq \theta \leq 60°$. Figure 11(a) shows the APS without the sample present. The symmetry of the signal indicates that the transmitter and receiver have relatively symmetric responses. The partial APS at the points labeled P on specimens A and B are shown in figures 11(b) and (c), respectively. The APS's are normalized to have a maximum amplitude of one. The APS for specimen A is relatively symmetric and indicates that this region is relatively free of porosity gradients. In contrast, the APS for specimen B is asymmetric and indicates the presence of porosity gradients. These gradients may be due to variations in the interlaminar bond at this point.

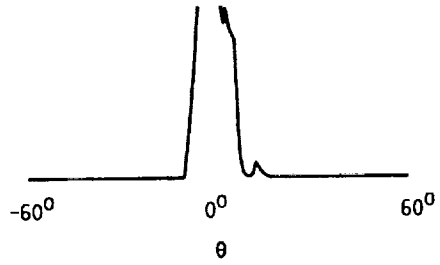

(a) SIGNAL WITHOUT SPECIMENS.

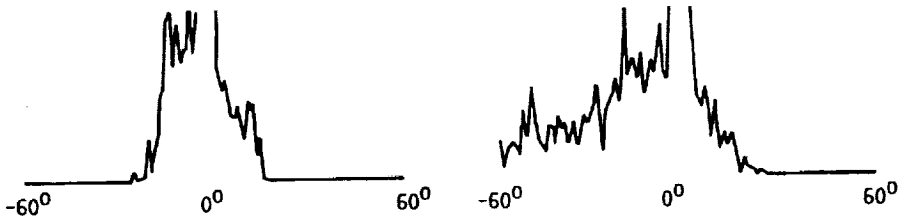

(b) SPECIMEN A: ALMOST SYMMETRIC AT POINT P.

(c) SPECIMEN B: ASYMMETRIC AT POINT P.

FIGURE 11. - PARTIAL ANGULAR POWER SPECTRUM (Φ = 0) FOR WOVEN COMPOSITES. (POINT P IS SHOWN IN FIG. 10.)

A quasi-APS was done by letting $\phi = 0°$, $-60° \leq \Theta \leq 60°$, and moving the receiving transducer along a line parallel to the specimen surface and along the Θ-axis of rotation. The resulting images are shown in figure 12. Figures 12(a) to (c) are quasi-APS images without the sample present, and for specimens A and B, respectively. A visual comparison between figures 11(b) and (c) dramatically reveals the presence and effect of asymmetric scattering detected by the APS technique.

(a) SIGNAL WITHOUT SPECIMEN.

(b) ALMOST SYMMETRIC AT POINT P FOR SPECIMEN A.

-60^0 60^0

(c) ASYMMETRIC AT POINT P FOR SPECIMEN B.

FIGURE 12. - QUASI-APS (ANGULAR POWER SPECTRUM WITH $\Phi = 0$) FOR WOVEN COMPOSITES. (POINT P IS SHOWN IN FIG. 10.)

REFERENCES

1. HITEMP Review 1989: Advanced High Temperature Engine Materials Technology Program. NASA CP-10039, 1989.

2. Structural Ceramics. NASA CP-2427, 1986.

3. Greil, P.; Petzow, G.; and Tanaka, H.: Sintering and HIPping of Silicon Nitride-Silicon Carbide Composite Materials. Ceram. Int., vol. 13, no. 1, 1987, pp. 19-25.

4. Nickel, K.G.; et al.: Thermodynamic Calculations for the Formation of SiC-Whisker-Reinforced Si_3N_4 Ceramics. Adv. Ceram. Mater., vol. 3, no. 6, Nov. 1988, pp. 557-562.

5. Freemann, M.R.; Kiser, J.D.; and Sanders, W.A.: A Sintering Model for SiC_w/Si_3N_4 Composites. NASA TM-101336, 1988.

6. Wei, G.C.; and Becher, P.F.: Development of SiC-Whisker-Reinforced Ceramics. Am. Ceram. Soc. Bull., vol. 64, no. 2, Feb. 1985, pp. 298-304.

7. Kobayashi, S.; Kandori, T.; and Wada, S.: Microstructure of Si_3N_4 Composites Reinforced with SiC Whiskers. J. Ceram. Soc. Jpn., vol. 94, no. 8, 1986, pp. 903-905.

8. Ishigaki, H.; et al.: Tribological Properties of SiC Whisker Containing Silicon Nitride Composite. J. Tribology, vol. 110, no. 3, July 1988, pp. 434-438.

9. Generazio, E.R.; and Roth, D.J.: Recent Advances in Nondestructive Evaluation Made Possible by Novel Uses of Video Systems. MiCon 90: Advances in Video Technology for Microstructural Control, ASTM STP-1094, George Van der Voort, ed., American Society for Testing and Materials, Philadelphia, May 23, 1990. (Also, NASA TM-102491).

10. Generazio, E.R.; Roth, D.J.; and Stang, D.B.: Ultrasonic Imaging of Porosity Variations Produced During Sintering, J. Am. Ceram. Soc., vol. 72, no. 7, July 1989, pp. 1282-1285.

11. Generazio, E.R.; Roth, D.J.; and Baaklini, G.Y.: Acoustic Imaging of, Subtle Porosity Variations in Ceramics. Mater. Eval., vol. 46, no. 10, Sept. 1988, pp. 1338-1343.

12. Generazio, E.R.: The Role of the Reflection Coefficient in Precision Measurement of Ultrasonic Attenuation. Mater. Eval., vol. 43, no. 8, July 1985, pp. 995-1004.

13. Generazio, E.R.; Stang, D.B.; and Roth, D.J.: Interfacing Laboratory Instruments to Multiuser, Virtual Memory Computers. Proceedings of The Sixteenth Annual Review of Progress in Quantitative Nondestructive Evaluation, vol. 9, D.O. Thompson and D.E. Chimenti, eds., Plenum Press, May 1990, pp. 1079-1085. (Also, NASA TM-4106).

14. Chou, C.H.; Khuri-Yakub, B.T.; and Kino, G.S.: Transmission Imaging: Forward Scattering and Scatter Reconstructing. Acoustical Imaging, vol. 9, Visualization and Characterization, K.Y. Wang, ed., Plenum Press, 1980, pp. 357-377.

15. Cooper, H.F., Jr.: Reflection and Transmission of Oblique Plane Waves at a Plane Interface Between Viscoelastic Media. J. Acoust. Soc. Am., vol. 42, no. 5, 1967, pp. 1064-1069.

16. Roth, D.J., et al.: Review and Statistical Analysis of the Ultrasonic Velocity Method for Estimating the Porosity Fraction in Polycrystalline Materials. NASA TM-102501, 1990.

17. Jenkins, F.A.; and White, H.E.: Fundamentals of Physical Optics. McGraw-Hill, 1937, Chapter 7.

NASA
National Aeronautics and Space Administration

Report Documentation Page

1. Report No.	2. Government Accession No.	3. Recipient's Catalog No.
NASA TM-102561		

4. Title and Subtitle	5. Report Date
Theory and Experimental Technique for Nondestructive Evaluation of Ceramic Composites	6. Performing Organization Code

7. Author(s)	8. Performing Organization Report No.
Edward R. Generazio	E-5381
	10. Work Unit No. 510-01-0A

9. Performing Organization Name and Address	11. Contract or Grant No.
National Aeronautics and Space Administration Lewis Research Center Cleveland, Ohio 44135-3191	13. Type of Report and Period Covered Technical Memorandum

12. Sponsoring Agency Name and Address	14. Sponsoring Agency Code
National Aeronautics and Space Administration Washington, D.C. 20546-0001	

15. Supplementary Notes

Prepared for the March Meeting of the American Society for Nondestructive Testing, Columbus, Ohio, March 15, 1990. Invited paper.

16. Abstract

The important ultrasonic scattering mechanisms for SiC and Si_3N_4 ceramic composites have been identified by examining the interaction of ultrasound with individual fibers, pores, and grains. The dominant scattering mechanisms have been identified as asymmetric refractive scattering due to porosity gradients in the matrix material, and symmetric diffractive scattering at the fiber-to-matrix interface and at individual pores. The effect of the ultrasonic reflection coefficient and surface roughness on the ultrasonic evaluation has been highlighted. A new nonintrusive ultrasonic evaluation technique, angular power spectrum scanning (APSS), has been presented that is sensitive to microstructural variations in composites. Preliminary results indicate that APSS will yield information on the composite microstructure that is not available by any other nondestructive technique.

17. Key Words (Suggested by Author(s))	18. Distribution Statement
Composites; Nondestructive evaluation; Ceramics; Ultrasonics; Porosity; Microstructure; NDE; NDT	Unclassified – Unlimited Subject Category 38

19. Security Classif. (of this report)	20. Security Classif. (of this page)	21. No. of pages	22. Price*
Unclassified	Unclassified	18	A03

NASA FORM 1626 OCT 86

*For sale by the National Technical Information Service, Springfield, Virginia 22161